Electronic Supplementary Material (ESI) for Physical Chemistry Chemical Physics.

Investigating the effect of ionic strength on the suppression of dendrite formation during metal electrodeposition

Supporting Information

Andrew K. Pearson[1], Pon Kao[2], Anthony P. O'Mullane,[3] Anand I. Bhatt*[2]*

[1] School of Chemistry, Monash University, Clayton, Melbourne, VIC 3001, Australia

[2] Energy Flagship, Commonwealth Scientific and Industrial Research Organisation (CSIRO), Clayton, Melbourne, Victoria 3169, Australia

[3] School of Chemistry, Physics and Mechanical Engineering, Queensland University of Technology (QUT), GPO Box 2434, QLD 4001, Australia.

*Corresponding authors: anthony.omullane@qut.edu.au and anand.bhatt@csiro.au

Additional SEM data

In order to probe the viscosity effect on dendrite growth further, SEM imaging of solutions of $AgNO_3$ in 0.1 mol L^{-1} KNO_3 were recorded. The aqueous solution viscosity was changed by addition of sucrose in 0, 20, 40 and 60 weight percent. Results obtained from deposition experiments are shown in Figure SI01:

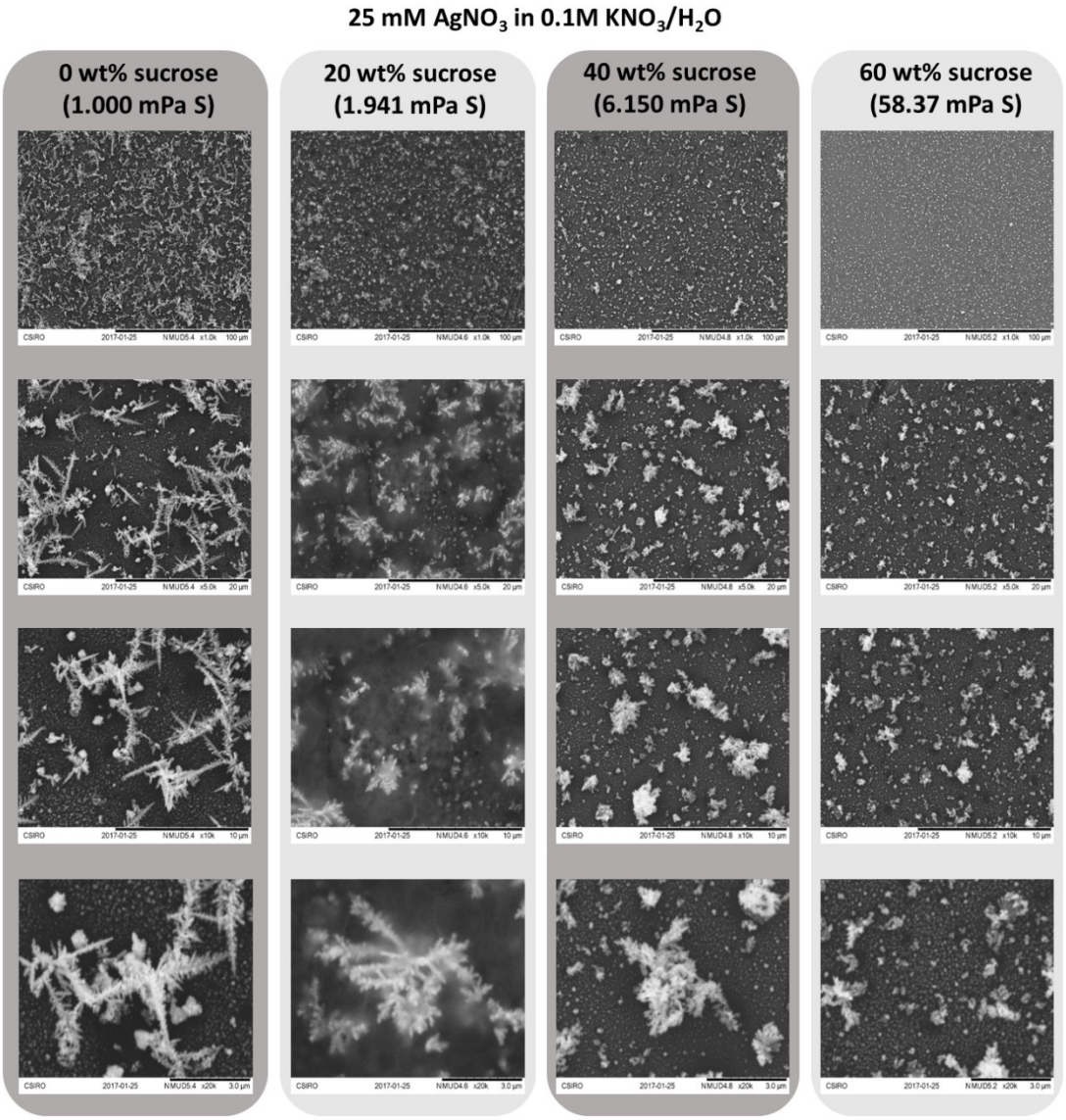

Figure SI01: SEM images of silver deposits from 25 mmol L^{-1}/$AgNO_3$/0.1mol L^{-1} KNO_3/water with added sucrose in the 0 to 60 wt% range to increase plating solution viscosity.

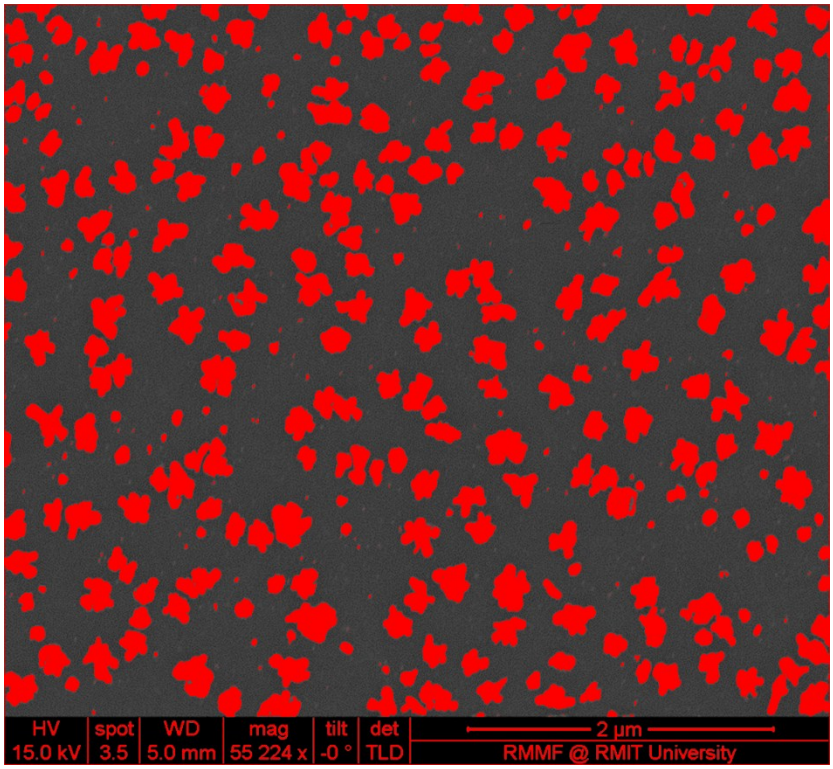

Figure SI02: False colour SEM image of silver deposits obtained from 25 mmol L^{-1} AgOTf in [EMIm][OTf] at -0.44V. Silver deposits are coloured in red.

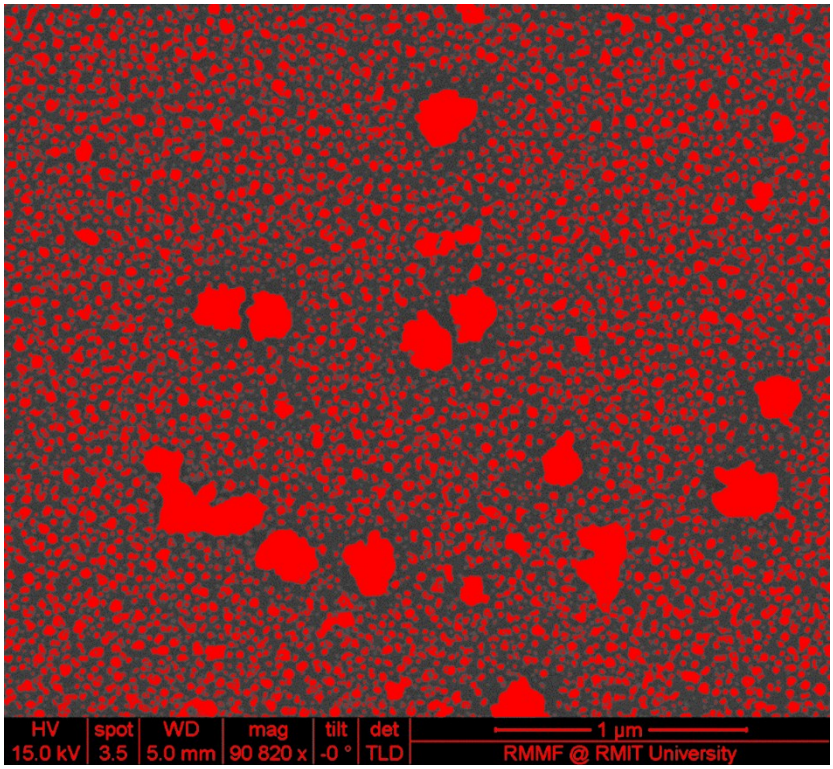

Figure SI03: False colour SEM image of silver deposits obtained from 25 mmol L^{-1} AgOTf in [EMIm][OTf] at -1.0V. Silver deposits are coloured in red.

Chronoamperometry measurements and data

Chronoamperometry is a technique commonly used to probe the nucleation and growth mechanisms during electrodeposition. In the present case, chronoamperograms were recorded at a GC working electrode where the potential was stepped from an initial value where no Ag deposition occurs to values close to, and beyond, E_p^{red} where Ag electrodeposition begins. On timescales of μs to ms, the initially high capacitive currents decay to give faradaic currents at longer timescales. The J-t curves recorded at E values close to E_p^{red} quickly reach a current maximum, J_m, at time t_m which then, at longer times, decays to a diffusion limited current. If the potential is stepped to values that are significantly more negative then E_p^{red} then the well-known $t^{-1/2}$ Cottrellian decay is observed.[1]

A number of models have been developed to describe this complex J-t behaviour for metal species being electrodeposited by nucleation and growth phenomena. The methodology developed by Hills and Scharifker[2] has previously been successfully employed for describing J-t transients for Pb and Ag deposition from ionic liquids[3,4] and Ag deposition from MeCN.[5] The Hills-Scharifker theory describes 2D nucleation and 3D growth mechanisms by two limiting cases. The first is instantaneous nucleation, where adatoms of metal are deposited and which subsequently grow at a uniform rate, dependent on applied potential. The second limiting case is where a progressive nucleation mechanism occurs whereby adatoms are continually deposited and grow at a non-uniform rate, which is dependent on applied potential and time of nucleation on electrode surface. The theoretical (dimensionless) current transients describing instantaneous and progressive growth are given by:[2]

For 2D instantaneous nucleation and 3D growth:

$$\left(\frac{J}{J_m}\right)^2 = \frac{1.9542}{t/t_m}\left\{1 - exp\left[-1.2564\left(\frac{t}{t_m}\right)\right]\right\}^2 \qquad \text{(Equation 1)}$$

For 2D progressive nucleation and 3D growth:

$$\left(\frac{J}{J_m}\right)^2 = \frac{1.2254}{t/t_m}\left\{1 - exp\left[-2.3367\left(\frac{t}{t_m}\right)^2\right]\right\}^2 \qquad \text{(Equation 2)}$$

Where, J = current density at time t and J_m = maximum current density at time t_m

Figure SI04 to SI10 shows typical plots of J-t obtained at different depositing voltages and the normalised J/J_m vs. t/t_m for Ag electrodeposition onto GC from the different ionic strength based electrolytes, and overlaid are the theoretical plots as calculated from Equations 1 and 2. Further analysis of the J-t curve using the Hills-Scharfiker theory can also provide information regarding the diffusion coefficient and the number of nuclei formed on the electrode surface as shown below:[2]

For instantaneous nucleation:

$$t_m = \frac{1.2564}{N\pi kD} \quad \text{(Equation 3)}$$

$$J_m = 0.6382nFDc(kN)^{1/2} \quad \text{(Equation 4)}$$

$$J_m^2 t_m = 0.1629(nFc)^2 D \quad \text{(Equation 5)}$$

where N = number of nuclei, D = diffusion coefficient, C_{bulk} = bulk concentration and k = $\left(\frac{8\pi C_{bulk} M}{\rho}\right)^{1/2}$ where, M = molar mass of the depositing species and ρ = density of depositing species.

And for Progressive nucleation:

$$t_m = \left(\frac{4.6733}{AN_\infty \pi k' D}\right)^{1/2} \quad \text{(Equation 6)}$$

$$J_m = 0.4615nFD^{3/4}c(k'AN_\infty)^{1/4} \quad \text{(Equation 7)}$$

$$J_m^2 t_m = 0.2598(nFc)^2 D \quad \text{(Equation 8)}$$

Where $k' = 4/3(8\pi cM/\rho)^{1/2}$ and A = steady state nucleation rate and N_∞ = number density of active sites

Results from analysis of the J-t curves using Equations 3-8 are presented in Supporting Information Table SI1 for the $TBAPF_6$/MeCN electrolyte system and Supporting information Table SI2 for the IL/MeCN system. It should be noted that a diagnostic criterion for nucleation and growth is that the product of $J_m^2 t_m$ is constant. As seen in the Tables, a small variance is observed in the $J_m^2 t_m$ and is attributed to low levels of uncompensated resistance, not fully accounted for by the potentiostat IR_u compensation features.

For the cases where instantaneous nucleation and growth is observed, the nuclei number density can be determined from Equations 4. However, for progressive nucleation and growth, Equations 6 and 7 only allow the product AN_∞, and not the nucleation number density N_0 directly, to be determined. It has been shown previously that the number density of nuclei formed has a dependence on the overpotential applied. Hills et al. have shown that the nucleation number density, N_0, can be calculated from the rising portion of the J-t curves using the following relationship:[6]

$$J = \frac{1.04nF\pi(2Dc)^{3/2}M^{1/2}N_0 t^{1/2}}{\rho^{1/2}} \quad \text{(Equation 9)}$$

Data for nuclei numbers calculated from the experimental data using Equations 4 and 9 is discussed further in the main manuscript.

E_p^{red}-E_{step} / V	t_m / s	J_m / A × 10^{-3} cm^{-2}	$J_m^2 t_m$ / × 10^{-5} A^2 cm^{-4} s	Nucleation number density × 10^5
0.1 mol L^{-1} $TBAPF_6$ in MeCN				
-0.138	2.96	4.43	5.8	27
-0.128	2.38	5.62	7.5	26
-0.098	1.34	7.84	8.2	43
-0.093	1.13	10.2	11.6	36
-0.088	1.02	10.7	11.7	39
-0.078	0.77	12.6	12.2	50
-0.068	1.38	6.35	5.6	62
-0.018	0.364	16.3	9.6	1.4
0.032	0.097	29.1	8.2	5.9
1 mol L^{-1} $TBAPF_6$ in MeCN				
-0.063	4.04	1.38	0.77	1.5
-0.053	2.62	2.11	1.2	1.5
-0.043	1.67	2.86	1.4	2.1
-0.033	1.22	3.75	1.7	2.3
-0.023	0.854	4.75	1.9	2.9
-0.013	0.796	5.73	2.6	2.3
-0.003	0.708	6.69	3.2	2.1
0.007	0.665	7.52	3.8	1.9
0.057	0.398	11.7	5.4	2.2
Saturated $TBAPF_6$ in MeCN				
-0.065	3.91	0.69	0.19	6.5
-0.055	2.17	1.19	0.31	7.1
-0.045	1.49	1.76	0.46	6.9
-0.035	1.20	2.27	0.61	6.4
-0.025	0.978	2.76	0.74	6.5
-0.015	0.789	3.35	0.89	6.7
-0.005	0.665	4.00	1.1	6.7
0.005	0.501	4.71	1.1	8.5

Table SI1: Experimental parameters for Ag deposition from $TBAPF_6$/MeCN electrolytes. Also shown N_0 values calculated using Equations 4 and 5.

E_p^{red}-E_{step} / V	t_m / s	J_m / A cm^{-2}	$J_m^2 t_m$ / A^2 cm^{-4} s	Nucleation number density	Mechanism type
0.1 mol L^{-1} [EMIm][OTf] in MeCN					
		× 10^{-3}	**× 10^{-4}**	**× 10^{4}**	
-0.065	5.23	2.51	0.33	2.7	Instantaneous
-0.055	3.89	3.23	0.41	3.0	Instantaneous
-0.045	2.79	4.87	0.67	2.6	Instantaneous
-0.035	2.20	6.86	1.0	2.1	Instantaneous
-0.025	1.92	7.79	1.2	2.1	Instantaneous
-0.015	1.68	9.84	1.6	1.7	Instantaneous
-0.005	1.36	11.8	1.9	1.8	Instantaneous
0.005	1.06	14.5	2.2	2.0	Instantaneous
0.015	0.777	17.9	2.5	2.4	Instantaneous
0.045	0.296	27.4	2.2	7.2	Instantaneous
1 mol L^{-1} [EMIm][OTf] in MeCN					
		× 10^{-3}	**× 10^{-5}**	**× 10^{5}**	
-0.059	4.17	4.16	7.2	7.3	Progressive
-0.054	2.49	4.62	5.3	35.6	Instantaneous
-0.049	1.92	4.91	4.6	52.8	Instantaneous
-0.044	1.60	5.34	4.6	64.7	Instantaneous
-0.039	1.25	5.96	4.4	85.2	Instantaneous
-0.034	1.01	6.79	4.7	99.6	Instantaneous
-0.029	0.873	7.41	4.8	1.1	Instantaneous
-0.024	0.803	7.95	5.1	1.2	Instantaneous
-0.019	0.711	8.54	5.2	1.3	Instantaneous
-0.014	0.617	9.31	5.4	1.4	Instantaneous
-0.009	0.546	9.98	5.4	1.6	Instantaneous
3 mol L^{-1} [EMIm][OTf] in MeCN					
		× 10^{-3}	**× 10^{-6}**	**× 10^{6}**	
-0.26	8.01	0.430	1.5	889	Progressive
-0.25	6.86	0.490	1.6	10.5	Progressive
-0.24	6.27	0.518	1.7	10.8	Progressive
-0.22	5.43	0.556	1.7	13.8	Progressive
-0.2	4.29	0.607	1.6	69.8	Instantaneous
-0.19	3.21	0.660	1.4	1.1	Instantaneous
-0.18	2.23	0.739	1.2	1.7	Instantaneous
-0.17	1.61	0.846	1.2	2.6	Instantaneous
-0.16	1.26	0.969	1.2	3.2	Instantaneous
-0.15	0.941	1.08	1.1	4.5	Instantaneous
-0.14	0.895	1.14	1.2	4.6	Instantaneous
-0.13	0.900	1.11	1.1	4.8	Instantaneous
-0.1	0.800	1.11	0.99	6.0	Instantaneous
[EMIm][OTf] only					
		× 10^{-4}	**× 10^{-7}**	**× 10^{7}**	
-0.308	10.766	2.33E-04	5.84E-07	0.031	Progressive
-0.258	3.919	3.79E-04	5.63E-07	0.24	Progressive
-0.208	1.987	5.26E-04	5.50E-07	0.97	Progressive
-0.158	1.329	7.73E-04	7.94E-07	1.5	Progressive
-0.108	1.109	7.75E-04	6.66E-07	2.6	Progressive

-0.058	0.817	8.54E-04	5.96E-07	5.3	Progressive
-0.008	0.506	1.04E-03	5.48E-07	14.9	Progressive
-0.042	0.297	1.62E-03	7.81E-07	30.4	Progressive

Table SI2: Experimental parameters for Ag deposition from [EMIm][OTf]/MeCN electrolytes. Also shown N_0 values calculated using Equations 4 and 5 or for progressive nucleation calculated using Equation 10.

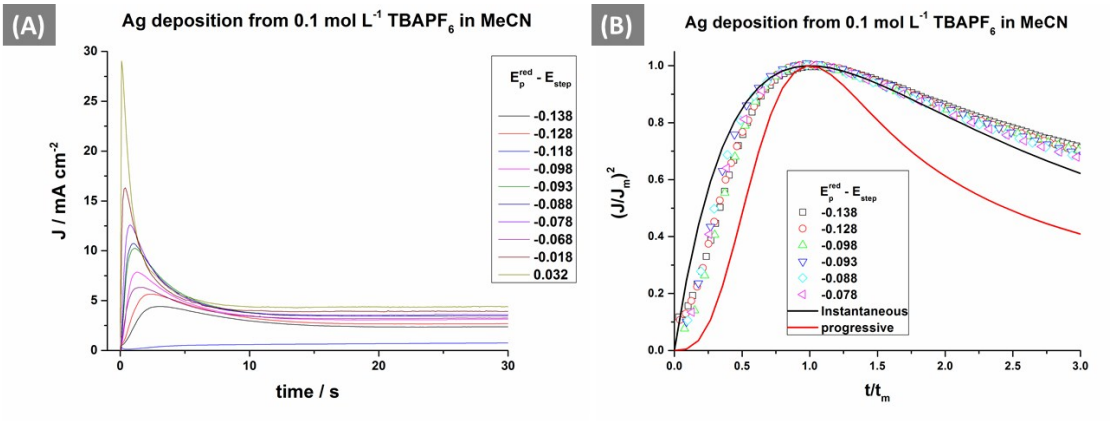

Figure SI04: (A) Chronoamperograms obtained as a function of step potential from a region where no deposition occurs up to the deposition peak voltage for 25 mmol L^{-1} AgOTf in 0.1 mol L^{-1} $TBAPF_6$ in MeCN; (B) Non-dimensional plots of $(J/J_m)^2$ vs t/t_m and overlayed are the theoretical curves calculated using Equations 1 and 2 for instantaneous (—) or progressive (••••) nucleation and diffusion limited growth.

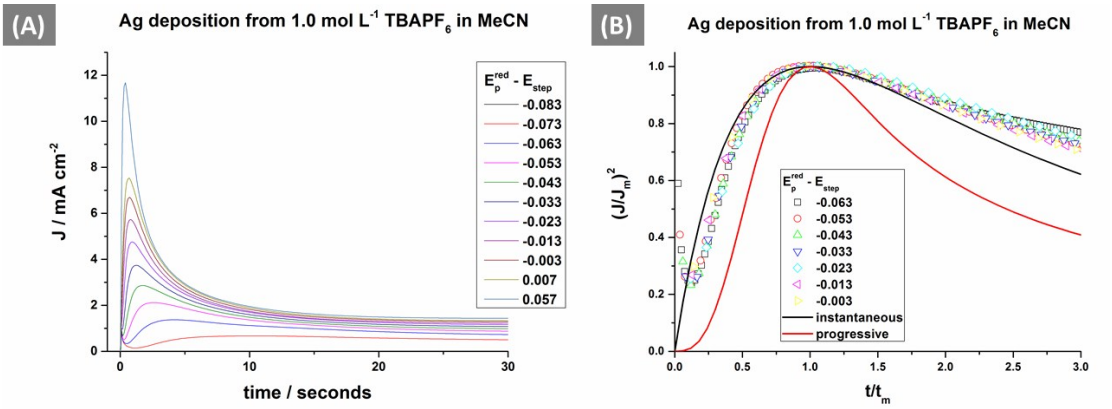

Figure SI05: (A) Chronoamperograms obtained as a function of step potential from a region where no deposition occurs up to the deposition peak voltage for 25 mmol L^{-1} AgOTf in 1 mol L^{-1} $TBAPF_6$ in MeCN; (B) Non-dimensional plots of $(J/J_m)^2$ vs t/t_m and overlayed are the theoretical curves calculated using Equations 1 and 2 for instantaneous (—) or progressive (••••) nucleation and diffusion limited growth.

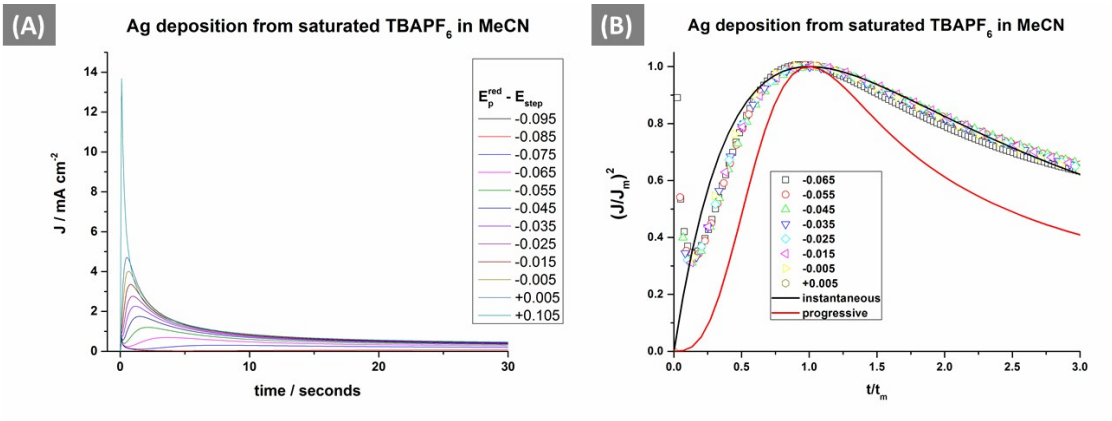

Figure SI06: (A) Chronoamperograms obtained as a function of step potential from a region where no deposition occurs up to the deposition peak voltage for 25 mmol L^{-1} AgOTf in saturated $TBAPF_6$ in MeCN; (B) Non-dimensional plots of $(J/J_m)^2$ vs t/t_m and overlayed are the theoretical curves calculated using Equations 1 and 2 for instantaneous (—) or progressive (••••) nucleation and diffusion limited growth.

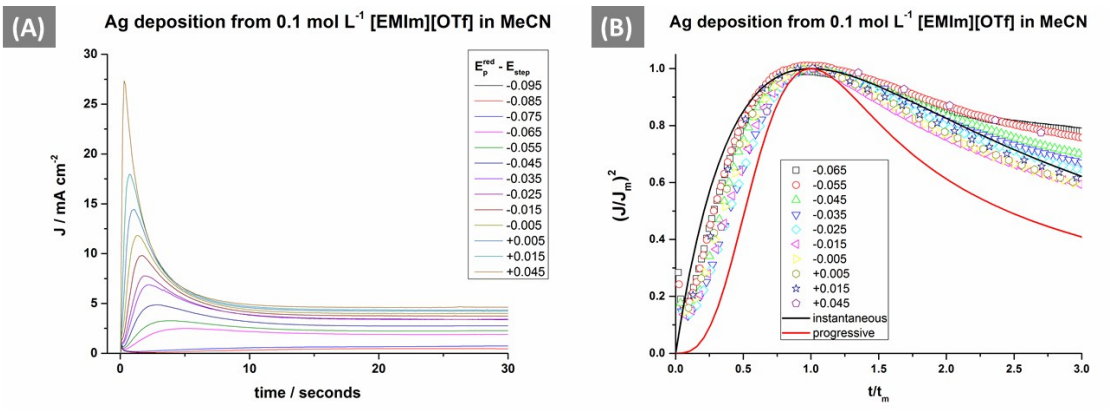

Figure SI07: (A) Chronoamperograms obtained as a function of step potential from a region where no deposition occurs up to the deposition peak voltage for 25 mmol L^{-1} AgOTf in 0.1 mol L^{-1} [EMIm][OTf] in MeCN; (B) Non-dimensional plots of $(J/J_m)^2$ vs t/t_m and overlayed are the theoretical curves calculated using Equations 1 and 2 for instantaneous (—) or progressive (••••) nucleation and diffusion limited growth.

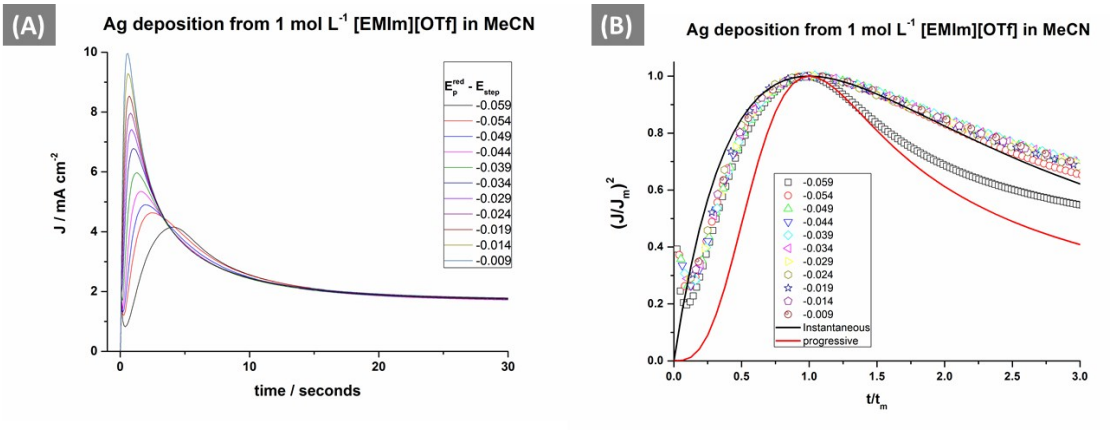

Figure SI08: (A) Chronoamperograms obtained as a function of step potential from a region where no deposition occurs up to the deposition peak voltage for 25 mmol L^{-1} AgOTf in 1 mol L^{-1} [EMIm][OTf] in MeCN; (B) Non-dimensional plots of $(J/J_m)^2$ vs t/t_m and overlayed are the theoretical curves calculated using Equations 1 and 2 for instantaneous (—) or progressive (••••) nucleation and diffusion limited growth.

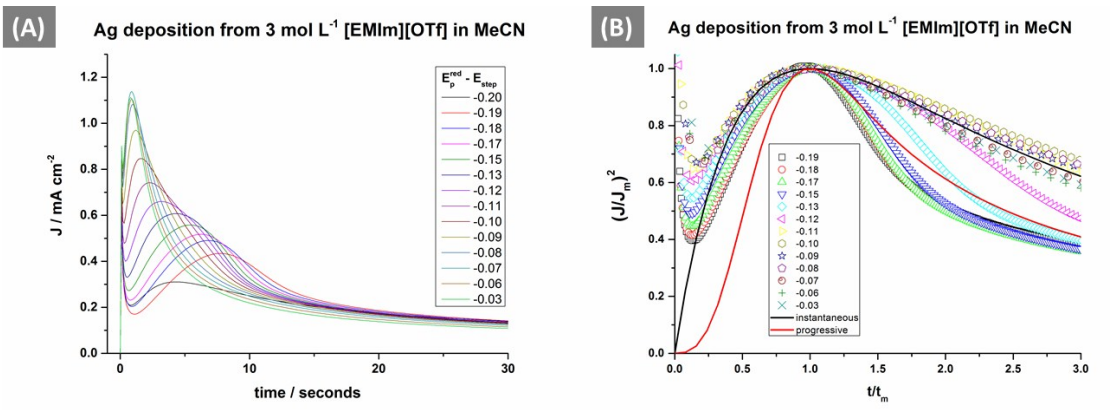

Figure SI09: (A) Chronoamperograms obtained as a function of step potential from a region where no deposition occurs up to the deposition peak voltage for 25 mmol L^{-1} AgOTf in 3 mol L^{-1} [EMIm][OTf] in MeCN; (B) Non-dimensional plots of $(J/J_m)^2$ vs t/t_m and overlayed are the theoretical curves calculated using Equations 1 and 2 for instantaneous (—) or progressive (••••) nucleation and diffusion limited growth.

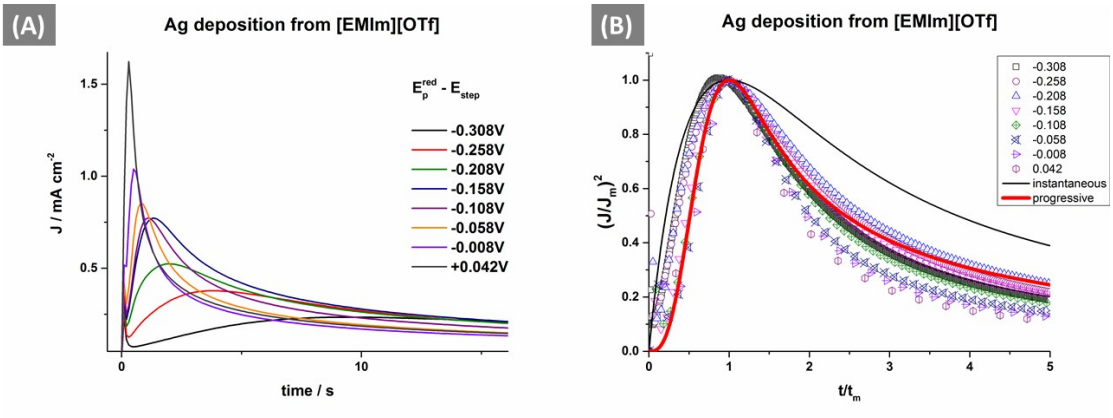

Figure SI10: (A) Chronoamperograms obtained as a function of step potential from a region where no deposition occurs up to the deposition peak voltage for 25 mmol L^{-1} AgOTf in [EMIm][OTf]; (B) Non-dimensional plots of $(J/J_m)^2$ vs t/t_m and overlayed are the theoretical curves calculated using Equations 1 and 2 for instantaneous (—) or progressive (••••) nucleation and diffusion limited growth.

Effect of temperature and concentration on silver electrodeposition

The effects of increasing the silver salt concentration on the voltammetry and morphology of the deposits was investigated for the 1 mol L^{-1} $TBAPF_6$/MeCN, 1 mol L^{-1} [EMIm][OTF]/MeCN and pure IL systems. AgOTf concentration was increased from 25 mmol L^{-1} to 0.25 mol L^{-1} (10 fold increase) and 0.5 mol L^{-1} (20 fold increase). All voltammograms obtained at 50 mV s^{-1} scan rate are shown in Figure SI11. In the case of 1M $TBAPF_6$/MeCN, at a AgOTf concentration of 0.25 mol L^{-1} and 0.5 mol L^{-1} (Figure SI11 A) the CVs show a broad reduction peak and a broad stripping peak. The peak-peak voltage difference (ΔE_p) is 321 mV. For the 0.5 mol L-1 AgOTf concentration, a (ΔE_p) value of 458 mV was observed. In addition for the highest AgOTf concentration, the appearance of a second peak at more negative voltages is also detected. Turning to the IL/MeCN system (Figure SI11 B), virtually identical voltammograms at both AgOTf concentrations are observed. Peak-peak separations of 427 mV (0.25 mol L^{-1}) and 500 mV (0.5 mol L^{-1}). The reason for this lack of concentration dependence on silver ion concentration is unknown at present and further investigations are underway. Finally for the pure [EMIm][OTf] (Figure SI11 C), silver stripping and plating peaks are observed at both concentrations with ΔE_p values of 544 mV (0.25 mol L^{-1}) and 612 mV (0.5 mol L^{-1}) obtained. The morphologies obtained for deposition from these systems are discussed in further details in the main manuscript.

For the [EMIm][OTf] system, voltammetry for 25 mmol L^{-1} AgOTf at 30 °C (Figure SI11 D), shows similar voltammetric features to the ambient temperature data. The main difference is that the peak current density has increased, suggestive of increased kinetics and/or mass transport. Similarly, further increasing the voltammetry temperature to 50 °C, further increases the current density and also decreased ΔE_p. the morphological changes associated with these conditions is discussed in the main manuscript and further investigations detailing these results and analysis will be presented at a later date.

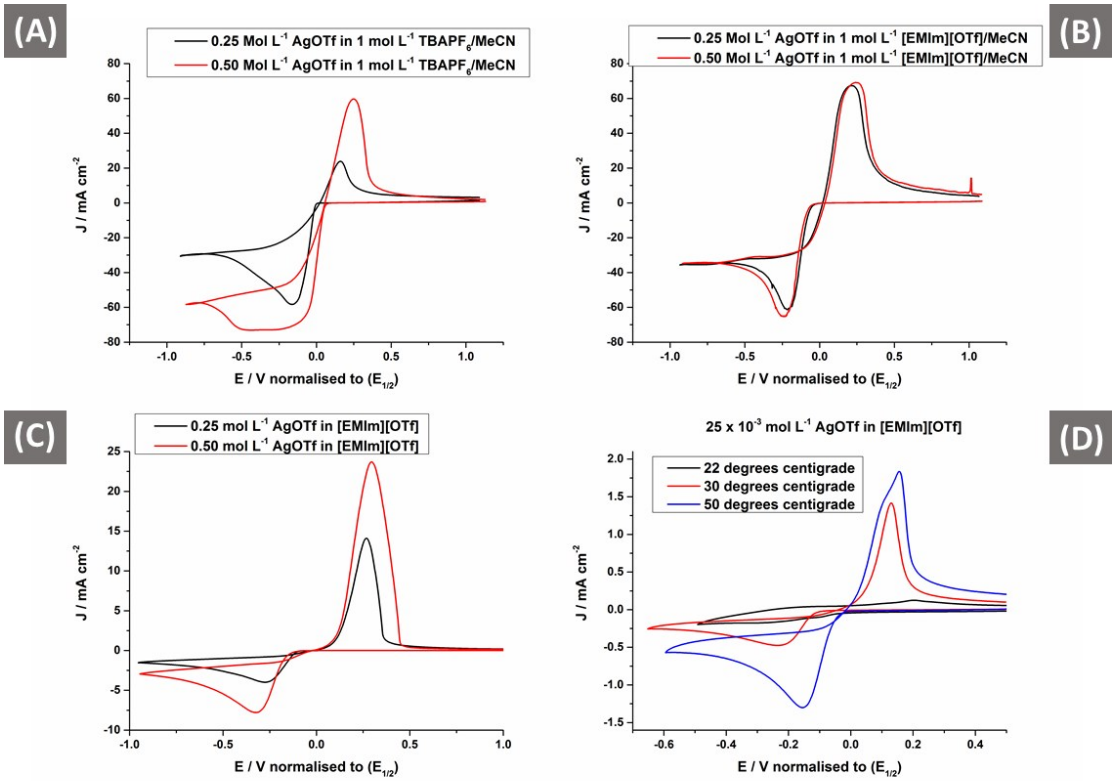

Figure SI11: (A) Cyclic voltammograms of silver deposition from 0.25 mol L^{-1} AgOTf (black) and 0.5 mol L^{-1} AgOTf (red) from 1 mol L^{-1} $TBAPF_6$ in MeCN; (B) silver deposition from 0.25 mol L^{-1} AgOTf (black) and 0.5 mol L^{-1} AgOTf (red) from 1 mol L^{-1} [EMIm][OTf] in MeCN; (C) silver deposition from 0.25 mol L^{-1} AgOTf (black) and 0.5 mol L^{-1} AgOTf (red) from [EMIm][OTf] and (D) cyclic voltammograms of silver deposition from 25 x 10× mol L^{-1} AgOTf from [EMIm][OTf] at 22 °C (black), 30 °C (red) and 50 °C (blue). All voltammograms recorded at a glassy carbon working electrode and for A-C recorded at 20 ± 2°C. To enable clarity between the different electrolyte systems, all CVs have been normalised by setting the $E_{1/2}$ for the $Ag^{0/+}$ process to zero volts.

Experimental

Materials and methods

Silver trifluoromethanesulphonate (AgOTf), Acetonitrile (MeCN), Sucrose and tetrabutylammonium hexafluorophosphate ($TBAPF_6$) were all purchased from Sigma Aldrich and used as received. Electrochemical grade ethyl-methyl imidazolium trifluoromethanesulphonate ([EMIm][OTf]) was purchased from IoLiTech and used as received. For saturated $TBAPF_6$/MeCN solutions, the limit of solubility of $TBAPF_6$ was measured at 9.90g in 10 mL solvent (i.e. 2.55 mol L^{-1}) and further additions resulted in solid particulates in the solution. The concentration of AgOTf in all electrolyte solutions was fixed at 25 × 10^{-3} mol L^{-1}.

Electrochemical measurements

Cyclic voltammetry and bulk electrodeposition experiments were conducted at 20 ± 2°C with a CH Instruments (CHI760C) electrochemical analyser in an electrochemical cell that allowed reproducible positioning of the working, reference, and auxiliary electrodes and a nitrogen inlet tube. A 0.196 cm^2 glassy carbon (GC) electrode, large surface area platinum counter electrode and a Ag/AgCl (3M KCl) reference electrode were used. Prior to electrodeposition the electrode was polished with an aqueous 0.3 μm alumina slurry on a polishing cloth (Microcloth, Buehler), thoroughly rinsed with MilliQ water, and dried with a flow of nitrogen gas.

Prior to bulk electrodeposition for SEM imaging, a CV was recorded to get the peak reduction current and peak reduction voltage for each electrolyte system. For electrodeposition, chronopotentiometry was performed at the peak current value obtained in the relevant cyclic voltammetric experiment until 0.0119C had been passed. The glassy carbon electrode was then removed from the electrolyte, washed three times with acetone and dried under a flow of nitrogen gas, prior to imaging.

Cyclic voltammetry and chronoamperometry studies were performed using an AutoLab PGSTAT302N potentiostat operated by GPES (ver. 4.9) software. All CV measurements were performed in a conventional three-electrode cell using a glassy carbon (0.0707 cm2) working electrode and a large surface area wound Pt wire counter electrode. For all electrochemical measurements, IR_u drop was compensated for using the Autolab potentiostat IRu compensation feature.

Physical characterisation

Scanning Electron Microscopy for all images presented in the main manuscript was performed on a FEI Nova NanoSEM at an operating voltage of 5-15kV. SEM images shown in Figure SI01 were recorded using a Hitachi TM3030PLUS at an operating voltage of 15kV. X-ray diffraction was performed on a Bruker AXS D8 Discover with General Area Detector Diffraction System (GADDS) using Cu Kα radiation of wavelength 1.54056 Å.

Supporting information references

1. A. J. Bard, L. R. Faulkner, *Electrochemical Methods: Fundamentals and Applications*, John Wiley & Sons Inc., New York, 2001.
2. B. Scharifker and G. Hill, *Electrochim. Acta*, **28**, 1983, 879-889.
3. A. I. Bhatt, A. M. Bond, J. Zhang, *J. Solid State Electrochem.*, **11**, 2007, 1593-1603.
4. C. L. Hussey and X. Xu, *J. Electrochem. Soc.*, **138**, 1991, 1886-1890.
5. C. Mele, S. Rondinini, L. D'Urzo, V. Romanello, E. Tondo, A. Minguzzi, A. Vertova, B. Bozzini, *J. Solid State Electrochem.*, **13**, 2009, 1577-1584.
6. G. A. Gunawardena, G. J. Hills, I. Montengro, *Electrochim. Acta*, **23**, 1978, 693-697 .